The Second-Order Bistatic High Frequency Radar Scattering Cross Section of the Ocean Surface for the Case of Floating Platform

Yue Ma, *Student Member, IEEE,* Weimin Huang, *Senior Member, IEEE*, Eric W. Gill, *Senior Member, IEEE*
Faculty of Engineering and Applied Science
Memorial University of Newfoundland, St. Johns, NL A1B 3X5, Canada

***Abstract*—The second-order bistatic high frequency radar cross section of ocean surface is derived for the case of a fixed receiver and a floating transmitter. The second-order radar cross section contains both the hydrodynamic contribution and the electromagnetic contribution. The second-order hydrodynamic contribution is obtained based on the first-order bistatic model with antenna motion. The derivation of the second-order electromagnetic contribution begins with a general expression for the bistatically received second-order electric field for the case of floating antenna. A new bistatic electromagnetic coupling coefficient, which unlike some earlier versions produces no non-physical singularities in the radar cross section, is derived. The new radar cross section model is simulated and compared with that of monostatic case. The motion-induced second-order peaks appearing in the spectrum are seen to have significantly less energy than those in the first-order case.**

I. Introduction

High frequency surface wave radar (HFSWR) has been successfully applied in ocean remote sensing for over four decades, and in more recent times attention has turned to bistatic operation. In particular, Walsh and Gill analyzed the scattering of high frequency electromagnetic radiation from rough surfaces [1]. Then, Gill and Walsh derived the bistatic form of the electric field equations and radar cross sections of the ocean surface in [2], [3]. Following those analyses, Gill *et al.* [4] developed a high frequency bistatic radar cross section for scatter from a patch of ocean. Later, Huang *et al.* [5] presented a technique to extract wind direction from the bistatic high frequency radar data.

While earlier HFSWR analyses focused on fixed antennas, interest in systems mounted on moving platforms has been increasing. In 2000, Gurgel and Essen [6] presented surface current measurements obtained from shipborne HF radar. Then, Xie *et al.* [7] investigated target detection using a shipborne HFSWR. Walsh *et al.* [8] proposed the monostatic model for the first-order high frequency radar cross section (HFRCS) for an antenna on a floating platform. In [9], a radar cross section model for a floating HFSWR was presented and the negative effects of antenna motion on the first-order Bragg lines were illustrated. Later, Walsh *et al.* derived the second-order monostatic model for patch scatter and foot scatter for a floating antenna in [10] and [11], respectively. This paper extends the work in [11] to include the bistatic case.

As in the various existing cross section models, the second-order bistatic radar cross section contains two portions: the hydrodynamic contribution and the electromagnetic contribution. The second-order hydrodynamic contribution is caused by the signal from the transmitter being scattered once by second-order ocean waves before being received. The second-order electromagnetic contribution arises from the double scattering from first-order ocean waves. It should be mentioned that only scatter scattering from a portion of the ocean surface which is remote from both the transmitter and receiver – the so-called patch scatter case – is addressed in this paper. This means that, for the double scatter case, the two scattering points are very close to each other compared to the distance between them and the antennas. The derivation of the hydrodynamic contribution is given in Section II. Section III contains the derivation of the electromagnetic contribution. The total second-order electric field equation and the bistatic radar patch scatter cross section are deduced in Section IV. Section V contains model simulations and the effects of various factors on the radar cross section are discussed. Conclusions and the direction for future work appear in Section VI.

II. The Second-Order Hydrodynamic Contribution

The first-order bistatic scattered field for the case of a floating transmitter and a fixed receiver appears in [12] as

$$
\begin{aligned}
(E_n)_1(t) = {} & \frac{-j\eta_0 \Delta l I_0 k_0^2}{(2\pi)^{3/2}} \sum_{\vec{K}} P_{\vec{K}} \sqrt{K\cos\phi_0} \\
& \cdot e^{j\frac{\rho K}{2}\cos(\theta_K-\theta)} e^{jk_0\Delta\rho_s} \\
& \cdot \frac{F(\rho_{02},\omega_0)F(\rho_{020},\omega_0)}{\sqrt{\rho_{0s}[\rho_{0s}^2-(\rho/2)^2]}} e^{-j\frac{\pi}{4}} e^{jK\rho_{0s}\cos\phi_0} \\
& \cdot e^{jK\delta\rho_0[\cos\phi_0\cos(\theta_K-\theta_0)+\sin\phi_0\sin(\theta_K-\theta_0)]/(2\cos\phi_0)} \\
& \cdot \Delta\rho_s Sa[\frac{\Delta\rho_s}{2}(\frac{K}{\cos\phi_0}-2k_0)]
\end{aligned}
\tag{1}
$$

with the various parameters and variables being identified as follows:

- η_0 represents the intrinsic impedance of free space;
- Δl is the length of the vertical dipole;
- I_0, ω_0 and k_0 are the peak current, the radian frequency and the wavenumber of the pulsed dipole, respectively;
- $P_{\vec{K}}$ is the Fourier coefficient of a surface component with its corresponding wave vector $\vec{K}=(K,\theta_K)$, K and θ_K being the magnitude and direction, respectively;

978-0-933957-43-5 ©2015 MTS

- $\vec{\rho}$ is a distance vector with the magnitude ρ and direction θ, pointing from transmitter to receiver;
- ρ_{02}, ρ_{020} and ρ_{0s} are the representative values of ρ_2, ρ_{20} and $\rho_s = \frac{\rho_1+\rho_2}{2}$, with ρ_2 and ρ_{20} being the distance from the transmitter to the first and the second scattering points, respectively;
- ϕ_0 is the representative bistatic angle, related to ρ_{0s};
- $\Delta\rho_s = \frac{c\tau}{2}$ is the patch width, depending on the radar pulse duration τ, and c is the free space speed of light;
- $\vec{\delta\rho}_0 = (\delta\rho_0, \theta_0)$ is the sway motion vector for the transmitter;
- F represents the Sommerfeld attenuation function;
- $Sa[x] = \sin(x)/x$.

The Fourier series for the second-order ocean waves can be expressed as [3]

$$P_{\vec{K},\omega} = \sum_{\substack{\vec{K}=\vec{K}_1+\vec{K}_2 \\ \omega=\omega_1+\omega_2}} {}_H\Gamma P_{\vec{K}_1,\omega_1} P_{\vec{K}_2,\omega_2} \tag{2}$$

where ${}_H\Gamma$ is the hydrodynamic coupling coefficient [13] accounting for the coupling of two first-order ocean waves, whose wave vectors and radian frequencies are $\vec{K}_1$, $\vec{K}_2$, ω_1 and ω_2, respectively. Using the time-varying ocean wave parameter $\xi(\vec{\rho},t) = \sum_{\vec{\rho},t} P_{\vec{K},\omega} e^{j\vec{K}\cdot\vec{\rho}} e^{j\omega t}$ with the second-order ocean waves Fourier series, shown as (2), to replace the time-invariant case $\xi(\vec{\rho}) = \sum_{\vec{\rho}} P_{\vec{K}} e^{j\vec{K}\cdot\vec{\rho}}$, (1) becomes

$$\begin{aligned}
{}_1(E_n)_2(t) = & \frac{-j\eta_0 \Delta l I_0 k_0^2}{(2\pi)^{3/2}} \sum_{\vec{K}_1,\omega_1} \sum_{\vec{K}_2,\omega_2} {}_H\Gamma P_{\vec{K}_1,\omega_1} \\
& \cdot P_{\vec{K}_2,\omega_2} e^{j(\omega_1+\omega_2)t} \sqrt{K\cos\phi_0}\, e^{j\frac{\rho K}{2}\cos(\theta_K-\theta)} \\
& \cdot e^{jk_0\Delta\rho_s} \frac{F(\rho_{02},\omega_0)F(\rho_{020},\omega_0)}{\sqrt{\rho_{0s}[\rho_{0s}^2-(\rho/2)^2]}} e^{-j\frac{\pi}{4}} e^{jK\rho_{0s}\cos\phi_0} \\
& \cdot e^{jK\delta\rho_0[\cos\phi_0\cos(\theta_K-\theta_0)+\sin\phi_0\sin(\theta_K-\theta_0)]/(2\cos\phi_0)} \\
& \cdot \Delta\rho_s Sa[\frac{\Delta\rho_s}{2}(\frac{K}{\cos\phi_0}-2k_0)].
\end{aligned} \tag{3}$$

III. The Second-Order Electromagnetic Contribution

A. General Second-Order Field Equation

Under the assumption of a good conducting surface and imposing the usual small height and small slope constraints for the ocean waves, the second-order HFSWR scattered field for a floating transmitter and a fixed receiver can be written as [10]

$$\begin{aligned}
(E_n)_2 \approx & \frac{k^2 C_0}{(2\pi)^3} \sum_{\vec{K}_1} \sum_{\vec{K}_2} P_{\vec{K}_1} P_{\vec{K}_2} \int_{A_1}\int_{A_2} (\vec{K}_1\cdot\hat{\rho}_1) \\
& \cdot (\vec{K}_2\cdot\hat{\rho}_{12}) e^{j\vec{K}_1\cdot\vec{\rho}_1} e^{j\vec{K}_2\cdot\vec{\rho}_2} e^{jk\hat{\rho}_1\cdot\vec{\delta\rho}_0} \\
& \cdot F(\rho_1)F(\rho_{12})F(\rho_{20}) \frac{e^{-jk(\rho_1+\rho_{12}+\rho_{20})}}{\rho_1\rho_{12}\rho_{20}} dA_1 dA_2.
\end{aligned} \tag{4}$$

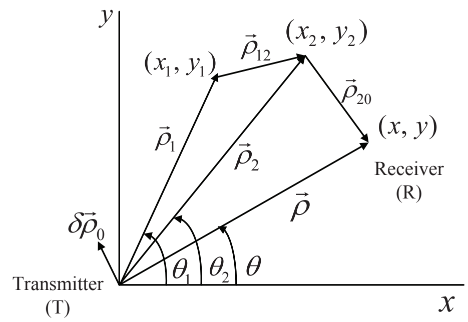

Fig. 1. Second-order bistatic scatter geometry with antenna motion

In Cartesian coordinate, $dA_1 = dx_1dy_1$ and $dA_2 = dx_2dy_2$. The dipole constant, C_0, is expressed as

$$C_0 = \frac{I\Delta l k^2}{j\omega\varepsilon_0}$$

where ε_0 is the permittivity of free space, I is the transmitter current with radian frequency ω and wavenumber k.

B. Patch Scatter Field Equation

Following the analyses in [1], [2] for patch scatter, it is clear that $\rho_{12} \ll \rho_1,\ \rho_2$. The geometry parameters are depicted in Fig. 1. By using the approximations $\rho_1 \approx \rho_2$ and $\theta_1 \approx \theta_2$ (the direction of $\vec{\rho_1}$ and $\vec{\rho_2}$, respectively) in the magnitude factor, (4) may be derived to be

$$\begin{aligned}
(E_n)_2 \approx & \frac{-kC_0}{(2\pi)^2} \sum_{\vec{K}_1} \sum_{\vec{K}_2} P_{\vec{K}_1} P_{\vec{K}_2} \\
& \cdot \int_{y_2}\int_{x_2} (-k\chi) \frac{F(\rho_2)F(\rho_{20})}{\rho_2\rho_{20}} e^{jk\hat{\rho}_2\cdot\vec{\delta\rho}_0} \\
& \cdot e^{-jk(\rho_2+\rho_{20})} e^{jK\rho_2\cos(\theta_K-\theta_2)} dx_2 dy_2
\end{aligned} \tag{5}$$

where $\vec{K} = \vec{K}_1 + \vec{K}_2$, with the magnitude K and direction θ_K. $\chi = j(\vec{K}_1\cdot\hat{\rho}_2)(\hat{K}_s\cdot\vec{K}_2)\cdot G[K_s(\hat{\rho}_2,\vec{K}_1)]$ where $\vec{K}_s(K_s,\ \theta_s) = k\hat{\rho}_2 - \vec{K}_1$ and

$$G[K_s(\hat{\rho}_2,\vec{K}_1)] = \frac{1}{K_s}\{1 - j\frac{k(1+\Delta)}{\sqrt{K_s^2-k^2}+jk\Delta}\}$$

where Δ is the intrinsic impedance of the surface.

As in [2], where the bistatic HF radar cross section for a stationary antenna was derived, by transforming the x-y coordinate system into the μ-δ elliptic coordinate (see Fig. 2) and applying a stationary phase method, a final asymptotic form for the bisticly received electric field may be written as

$$\begin{aligned}
(E_n)_2 = & \frac{-kC_0}{(2\pi)^{\frac{3}{2}}} \sum_{\vec{K}_1} \sum_{\vec{K}_2} \frac{P_{\vec{K}_1}P_{\vec{K}_2}}{\sqrt{K}} e^{j\frac{\rho}{2}K\cos(\theta_K-\theta)} e^{\mp j\frac{\pi}{4}} \\
& \cdot \int_{\frac{\rho}{2}}^{\infty} \frac{(-k\chi)F(\rho_2)F(\rho_{20})}{\sqrt{\cos\phi}} \frac{e^{j\rho_s(\pm K\cos\phi-2k)}}{\sqrt{\rho_s(\rho_s^2-(\frac{\rho}{2})^2)}} \\
& \cdot e^{jk\delta\rho_0[\cos\phi\cos(\theta_K-\theta_0)+\sin\phi\sin(\theta_K-\theta_0)]} d\rho_s
\end{aligned} \tag{6}$$

where $\rho_s = \frac{\rho_2+\rho_{20}}{2}$. The bistatic angle ϕ, shown in Fig. 2, bisects the angle between $\vec{\rho}_1$ and $\vec{\rho}_{20}$ [14]. It is also shown in [14] that for second-order patch scatter $\theta_K = \theta_N$, where θ_N is the direction of the scattering ellipse normal.

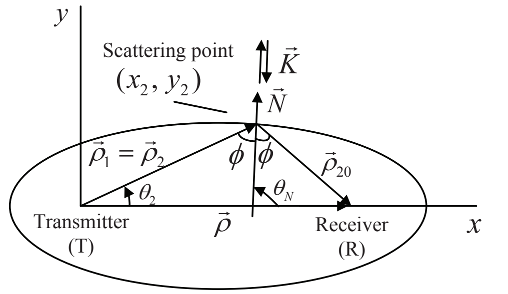

Fig. 2. Geometry associated with the second-order stationary phase condition. T and R are the foci of the scattering ellipse.

C. Pulsed Radar Field Equation

Following the analysis given for a pulsed dipole source in [3], [12] and taking the inverse Fourier transform of (6), the time domain result for the second-order electric field is

$$\begin{aligned}(E_n)_2(t) = &\frac{-j\eta_0 \Delta l I_0 k_0^2}{(2\pi)^{3/2}} \sum_{\vec{K}_1} \sum_{\vec{K}_2} {}_E\Gamma_P P_{\vec{K}_1} P_{\vec{K}_2} \\ &\cdot e^{j\frac{\rho K}{2}\cos(\theta_K - \theta)} e^{jk_0 \Delta\rho_s} \sqrt{K\cos\phi_0} \\ &\cdot \frac{F(\rho_{02},\omega_0)F(\rho_{020},\omega_0)e^{-j\frac{\pi}{4}}}{\sqrt{\rho_{0s}(\rho_{0s}^2 - (\frac{\rho}{2})^2)}} e^{jK\rho_{0s}\cos\phi_0} \\ &\cdot e^{jK\delta\rho_0[\cos\phi_0\cos(\theta_K-\theta_0)+\sin\phi_0\sin(\theta_K-\theta_0)]/(2\cos\phi_0)} \\ &\cdot \Delta\rho_s Sa[\frac{\Delta\rho_s}{2}(\frac{K}{\cos\phi_0} - 2k_0)]\end{aligned} \tag{7}$$

where ${}_E\Gamma_P = \frac{k_0\chi}{K\cos\phi_0}$ is the electromagnetic coupling coefficient. Replacing the time-invariant rough surface by the time-varying ocean surface, (7) can be written as

$$\begin{aligned}&(E_n)_2(t) \\ &= \frac{-j\eta_0 \Delta l I_0 k_0^2}{(2\pi)^{3/2}} \sum_{\vec{K}_1,\omega_1} \sum_{\vec{K}_2,\omega_2} {}_{SE}\Gamma_P P_{\vec{K}_1,\omega_1} P_{\vec{K}_2,\omega_2} \\ &\cdot e^{j(\omega_1+\omega_2)t} \sqrt{K\cos\phi_0} e^{j\frac{\rho K}{2}\cos(\theta_K - \theta)} e^{jk_0\Delta\rho_s} \\ &\cdot \frac{F(\rho_{02},\omega_0)F(\rho_{020},\omega_0)}{\sqrt{\rho_{0s}[\rho_{0s}^2 - (\rho/2)^2]}} e^{-j\frac{\pi}{4}} e^{jK\rho_{0s}\cos\phi_0} \\ &\cdot e^{jK\delta\rho_0[\cos\phi_0\cos(\theta_K-\theta_0)+\sin\phi_0\sin(\theta_K-\theta_0)]/(2\cos\phi_0)} \\ &\cdot \Delta\rho_s Sa[\frac{\Delta\rho_s}{2}(\frac{K}{\cos\phi_0} - 2k_0)]\end{aligned} \tag{8}$$

where an expression for the symmetrical electromagnetic coupling coefficient can be written as

$$\begin{aligned}&{}_{SE}\Gamma_P(\vec{K}_1, \vec{K}_2) \\ &= \frac{1}{2}[{}_E\Gamma_P(\vec{K}_1,\vec{K}_2) +_E \Gamma_P(\vec{K}_2,\vec{K}_1)] \\ &= \frac{jk_0}{2K\cos\phi_0}\{(\vec{K}_1\cdot\hat{\rho}_2) \\ &\cdot [\hat{K}_s(\hat{\rho}_2,\vec{K}_1)\cdot\vec{K}_2] G[K_s(\hat{\rho}_2,\vec{K}_1)] \\ &+ (\vec{K}_2\cdot\hat{\rho}_2)[\hat{K}_s(\hat{\rho}_2,\vec{K}_2)\cdot\vec{K}_1] G[K_s(\hat{\rho}_2,\vec{K}_2)]\}\end{aligned} \tag{9}$$

with $\vec{K}_s(\hat{\rho}_2, \vec{K}_2) = k\hat{\rho}_2 - \vec{K}_2$.

IV. Second-Order Radar Cross Section For Patch Scatter

From (3) and (8), the total second-order scattering field, including both the electromagnetic portion and the hydrodynamic portion, can be expressed as

$$\begin{aligned}(E_n)_{2P}(t) &= {}_1(E_n)_2(t) + (E_n)_2(t) \\ &= \frac{-j\eta_0 \Delta l I_0 k_0^2}{(2\pi)^{3/2}} \sum_{\vec{K}_1,\omega_1} \sum_{\vec{K}_2,\omega_2} \Gamma_P P_{\vec{K}_1,\omega_1} P_{\vec{K}_2,\omega_2} \\ &\cdot e^{j(\omega_1+\omega_2)t} \sqrt{K\cos\phi_0} e^{j\frac{\rho K}{2}\cos(\theta_K - \theta)} e^{jk_0\Delta\rho_s} \\ &\cdot \frac{F(\rho_{02},\omega_0)F(\rho_{020},\omega_0)}{\sqrt{\rho_{0s}[\rho_{0s}^2 - (\rho/2)^2]}} e^{-j\frac{\pi}{4}} e^{jK\rho_{0s}\cos\phi_0} \\ &\cdot e^{jK\delta\rho_0[\cos\phi_0\cos(\theta_K-\theta_0)+\sin\phi_0\sin(\theta_K-\theta_0)]/(2\cos\phi_0)} \\ &\cdot \Delta\rho_s Sa[\frac{\Delta\rho_s}{2}(\frac{K}{\cos\phi_0} - 2k_0)]\end{aligned} \tag{10}$$

where $\Gamma_P = {}_{SE}\Gamma_P + {}_H\Gamma$. A similar process, as was used in [3], [12], is used to obtain the radar cross section from the electric field equation. The initial step of the approach is to write the autocorrelation, $R_{2P}(\tau)$, as

$$R_{2P}(\tau) = \frac{A_r}{2\eta_0} < (E_n^+)_{2P}(t_0, t+\tau)(E_n^+)_{2P}^*(t_0, t) > \tag{11}$$

where $A_r = (\lambda_0^2/4\pi)G_r$, with G_r being the gain of the receiving array; τ represents the interval between samples and $*$ indicates complex conjugation.

In keeping with [10], it is assumed that the sway motion $\vec{\delta\rho_0} = a\sin(\omega_p t)\hat{\rho}_p$, which is caused by the dominant ocean wave. The sway frequency can be expressed as $\omega_p = \sqrt{gK_p}$, where K_p is the dominant ocean wavenumber, and a is the sway amplitude depending on the sea state. In addition, ω_p and a are assumed to be constant during the sets of observations. The direction of $\vec{\delta\rho_0}$ is represented by the hatted vector $\hat{\rho}_p$ or θ_{K_p}.

After Fourier transforming the autocorrelation and comparing directly with the radar range equation, the radar cross section, $\sigma_{2P}(\omega_d)$, may be written as

$$\begin{aligned}\sigma_{2P}(\omega_d) = &2^3\pi k_0^2 \Delta\rho_s \sum_{m_1=\pm1}\sum_{m_2=\pm1}\int_0^\infty\int_{-\pi}^{\pi}\int_0^\infty \\ &\cdot\{S_1(m_1\vec{K}_1)S_1(m_2\vec{K}_2)|_s\Gamma_P|^2 K^2 K_1\cos\phi_0 \\ &\cdot Sa^2[\frac{\Delta\rho_S}{2}(\frac{K}{\cos\phi_0} - 2k_0)] \\ &\cdot\{J_0^2\{\frac{aK}{2}|\cos(\theta_K - \theta_{K_p}) + \tan\phi_0\sin(\theta_K - \theta_{K_p})|\} \\ &\cdot\delta(\omega_d + m_1\sqrt{gK_1} + m_2\sqrt{gK_2}) \\ &+\sum_{n=1}^{\infty} J_n^2\{\frac{aK}{2}|\cos(\theta_K - \theta_{K_p}) + \tan\phi_0\sin(\theta_K - \theta_{K_p})|\} \\ &\cdot[\delta(\omega_d + m_1\sqrt{gK_1} + m_2\sqrt{gK_2} - n\omega_p) \\ &+\delta(\omega_d + m_1\sqrt{gK_1} + m_2\sqrt{gK_2} + n\omega_p)]\} \\ &\cdot dK_1 d\theta_{\vec{K}_1} dK\}\end{aligned} \tag{12}$$

where ω_d represents the radian Doppler frequency. $S_1(\vec{K})$ indicates the spectrum of the first-order ocean surface waves and δ is the Dirac delta function. The J_n are Bessel functions of order n.

Equation (12) is the final result for the second-order bistatic radar patch scatter cross section with a floating transmitter and a fixed receiver. If there is no antenna motion (i.e. $\delta\vec{\rho}_0 = 0$), the radar cross section reduces to that of the case with both transmitter and receiver fixed shown in [3]. If the bistatic angle ϕ_0 is taken to be 0, then the bistatic cross section can be shown to reduce to that of monostatic swaying antenna case.

V. Simulation and Discussion

A technique similar to that in [14], [15] is used to compute the radar cross sections. Based on a Pierson-Moskowitz (PM) spectral model [16], the simulation result is shown in Fig. 3 to illustrate the relative contributions of the second-order hydrodynamic and electromagnetic radar cross sections as well as the peaks caused by antenna motion. The operating frequency is 15 MHz, the bistatic angle is 30° and the wind speed is 20 knots. The ellipse normal and the wind direction are 90° and 180°, respectively, as measured from the positive x axis (the line connecting the transmitter with the receiver), respectively. In keeping with [10], [12], the platform sway is assumed to be due to the dominant ocean wave. The sway amplitude and frequency depend on the wind velocity and are given in Table I in [8]. The sway direction is chosen to be the same as the wind direction.

Fig. 3(a) and Fig. 3(b) show the second-order hydrodynamic results without and with antenna motion, respectively. $h1$ represents the hydrodynamic peak at Doppler frequency $\pm\sqrt{2}\omega_B$. The physical meaning of this peak is a single scatter from a second-order ocean surface component of wave length λ_B. From Fig. 3(b), extra hydrodynamic peaks $h2$ at $\pm\sqrt{2}\omega_B \pm \omega_p$ due to the platform motion are observed. Fig. 3(c) and Fig. 3(d) depict the second-order electromagnetic results without and with antenna motion, respectively. $e1$ and $e2$ occur for [14]

$$K_1 = K_2$$

and

$$\omega_d = \pm 2^{\frac{3}{4}} \sqrt{\frac{[1 \pm \sin\phi_0]^{\frac{1}{2}}}{\cos\phi_0}}\,\omega_B.$$

For monostatic operation, (i.e. $\phi_0 = 0$), the four peaks are reduced to two peaks at $\omega_d = \pm 2^{\frac{3}{4}}\omega_B$, which is the well known 'corner reflector'. From Fig. 3(d), it can be seen that the electromagnetic peaks are shifted by $\pm\omega_p$. In these figures, motion effects may be considered only up to second-order for the first-order radar cross section and up to first-order for the second-order radar cross section. This is because the energy of the motion-induced peaks in the second-order radar cross section is relatively lower than that of the first-order result. In total, the second-order hydrodynamic contribution is greater than that of the electromagnetic. The discussion regarding the first-order bistatic result for the case with a floating transmitter and a fixed receiver can be found in [12]. The total bistatic radar patch scatter cross sections for stationary antennas and floating antennas are shown in Fig. 3(e) and Fig. 3(f), respectively.

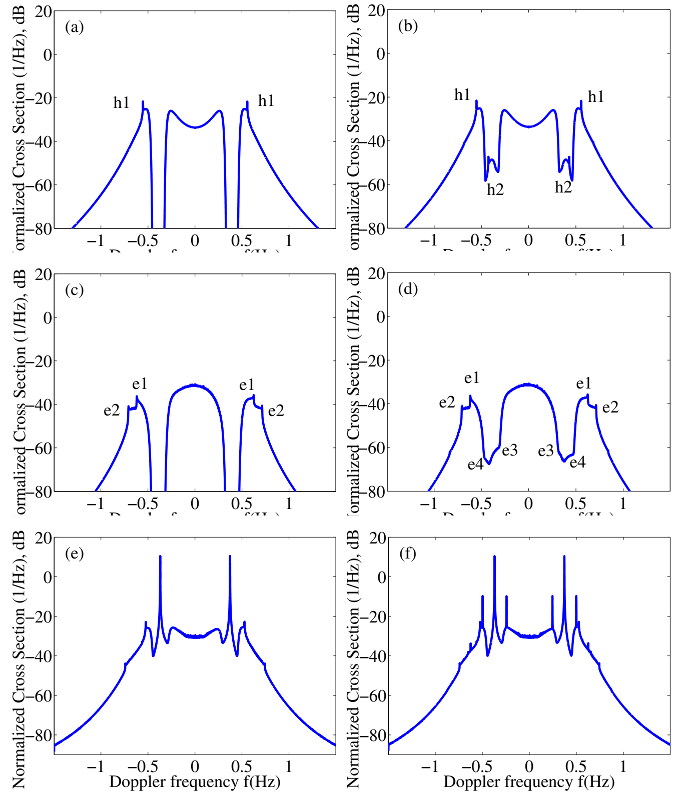

Fig. 3. (a) the second-order bistatic hydrodynamic contribution without antenna motion. (b) the second-order hydrodynamic contribution without antenna motion. (c) the second-order electromagnetic contribution without antenna motion. (d) the second-order electromagnetic contribution with antenna motion. (e) the total bistatic radar cross section without antenna motion. (f) the total bistatic radar cross section with antenna motion.

The difference between the bistatic and monostatic radar cross sections with antenna motion is depicted in Fig. 4. Keeping the location of the transmitter and the wind direction fixed, comparison is made by varying the antenna operating geometry (bistatic or monostatic). By comparison, it can be seen that the frequencies of the first-order and the second-order peaks are closer to zero Doppler frequency in the bistatic case than those in the monostatic case. This is also true for peaks induced by the platform motion. It may be observed that in the monostatic case, the peaks (including the Bragg peaks and the motion-induced peaks) in the negative Doppler frequency region have less energy, while the peaks in the positive Doppler frequency region have more energy than those of bistatic case. This is because, for the example chosen here, the angle between the wind direction with the look direction θ_L in the monostatic case is larger than the angle between the wind direction with the ellipse normal θ_N in the bistatic case.

VI. Conclusion

The development of the second-order bistatic radar patch scatter cross section of the ocean surface has been presented for the case of a fixed receiver and a transmitter being mounted on a floating platform. Both the hydrodynamic and the electromagnetic contributions are derived. The hydrodynamic contribution has singularities at $\pm\sqrt{2}\omega_B$, while the modified

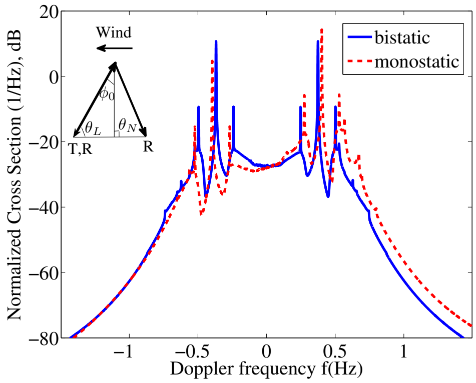

Fig. 4. Compare the radar cross sections with floating platform for the bistatic case with bistatic angle of 30° and for the monostatic case. Wind direction is 180°, ellipse normal $\theta_N = 90°$ for bistatic geometry and look direction $\theta_L = 60°$ for monostatic geometry.

electromagnetic coupling coefficient produces no non-physical singularities. Based on the new model, simulations have been made to illustrate the effect of motion-induced peaks on the radar cross section and to compare the bistatic model with the monostatic case. It is found that sway-motion-induced peaks appear in the Doppler spectrum and are more significant in the first-order radar cross section than that in the second-order case.

This analysis presented here for pulsed radars is currently being extended to frequency-modulated continuous-wave (FMCW) systems which presently are in widespread use in ocean remote sensing.

Acknowledgment

The authors would like to thank B. Dawe of Northern Radar Inc. for providing typical platform motion data. The work was supported in part by Natural Sciences and Engineering Research Council of Canada (NSERC) under Grants to W. Huang (NSERC 402313-2012) and E. W. Gill (NSERC RGPIN-2015-05289) and by an Atlantic Innovation Fund Award (E. W. Gill, principal investigator). The work was also supported by the Department of Innovation, Business and Rural Development of Newfoundland and Labrador under Grant 30-10921-008 to E. W. Gill and W. Huang.

References

[1] J. Walsh and E. W. Gill, "An analysis of the scattering of high-frequency electromagnetic radiation from rough surfaces with application to pulse radar operating in backscatter mode," *Radio Sci.*, vol. 35, no. 6, pp. 1337-1359, 2000.

[2] E. W. Gill and J. Walsh, "Bistatic form of the electric field equations for the scattering of vertically polarized high frequency ground wave radiation from slightly rough, good conducting surfaces," *Radio Sci.*, vol. 35, no. 6, pp. 1323-1335, 2000.

[3] E. W. Gill and J. Walsh, "High-frequency bistatic cross sections of the ocean surface," *Radio Sci.*, vol. 36, no. 6, pp. 1459-1475, 2001.

[4] E. Gill, W. Huang, and J. Walsh, "On the development of a second-order bistatic radar cross section of ocean surface: A high-frequency result for a finite scattering patch," *IEEE J. Oceanic Eng. Special Issue on HF/VHF Sea Surface Radar*, vol. 31, no. 4, pp. 740-750, 2006.

[5] W. Huang, E. Gill, X. Wu, and L. Li, "Measurement of sea surface wind direction using bistatic high-frequency radar," *IEEE Trans. Geosci. Remote Sens.*, vol. 50, no. 10, pp. 4117-4122, 2012.

[6] K. W. Gurgel and H. H. Essen, "On the performance of a shipborne current mapping HF radar," *IEEE J. Oceanic Eng.*, vol. 25, no. 1, pp. 183-191, 2000.

[7] J. Xie, Y. Yuan, and Y. Liu, "Suppression of sea clutter with orthogonal weighting for target detection in shipborne HFSWR", *IET Radar Sonar Navig.*, vol. 149, no. 1, pp. 39-44, 2012.

[8] J. Walsh, W. Huang, and E. Gill, "The first-order high frequency radar ocean surface cross section for an antenna on a floating platform," *IEEE Trans. Antennas Propaga.*, vol. 58, no. 9, pp. 2994-3003, 2010.

[9] J. El Khoury, R. Guinvarch, R. Gillard, and B. Uguen, "Sea-echo doppler spectrum perturbation of the received signals from a floating high-frequency surface wave radar," *IET Radar Sonar Navig.*, vol. 6, no. 3, pp. 165-171, 2012.

[10] J. Walsh, W. Huang, and E. Gill, "The second-order high frequency radar ocean surface cross section for an antenna on a floating platform," *IEEE Trans. Antennas Propag.*, vol. 60, no. 10, pp. 4804-4813, 2012.

[11] J. Walsh, W. Huang, and E. Gill, "The second-order high frequency radar ocean surface foot-scatter cross section for an antenna on a floating platform," *IEEE Trans. Antennas Propag.*, vol. 61, no. 11, pp. 5833-5838, 2013.

[12] Y. Ma, E. W. Gill, and W. Huang, "The First-Order Bistatic High Frequency Radar Scattering Cross Section of the Ocean Surface for the Case of a Floating Platform," in *Proceedings of MTS/IEEE OCEANS Conference* - Genova, Italy, May 2015.

[13] K. Hasselmann, "On the nonlinear energy transfer in a gravity wave spectrum, part 1, general theory," *J. Fluid Mech.*, vol. 12, pp. 481-500, 1962.

[14] Gill, E., "The scattering of high frequency electromagnetic radiation from the ocean surface: An analysis based on a bistatic ground wave radar configuration," Ph.D. thesis, Mem. Univ. of Newfoundland, St. Johns, Newfoundland, Canada, 1999.

[15] B. J. Lipa and D. E. Barrick, "Extraction of sea state from HF radar sea echo: Mathematical theory and modelling," *Radio Sci.*, vol. 21, no. 1, pp. 81-100, 1986.

[16] W. Pierson and L. Moskowiz, "A proposed spectral form for fully developed seas based upon the similarity theory of S. A. Kitaigorodskii," *J. Geophys. Res.*, vol. 69, pp. 5181-5190, 1964.